ICAS 2021 SHANG HAI
International Council of the Aeronautical Sciences
32nd Congress of the International Council of the Aeronautical Sciences
September 6-10, 2021 Pudong Shangri-La, Shanghai, China

NUMERICAL SIMULATION OF PITCHING MOTION EFFECTS ON THE AERODYNAMIC PERFORMANCE OF DRAGONFLY-LIKE FLAPPING WING

Xinyu Lang, Bifeng Song, Wenqing Yang

School of Aeronautics, Northwestern Polytechnical University, Xi'an 710072, China

Abstract

Dragonflies have remarkable flight skills and their excellent flight performance has attracted persistent attention. The multi-degree-of-freedom flapping kinematics and interaction of the tandem wings might account for their extraordinary flight skills. In this paper, the effects of pitching motion on the aerodynamic performance of a dragonfly-like flapping wing have been numerically studied. A transient numerical method based on the overset mesh technique is used to simulate the flapping and pitching movements. Different pitching amplitudes have been evaluated as the forewing and hindwing flap in counter-stroking during the hovering process. It is found that the pitching motion has an obvious influence on the tandem wings' aerodynamic performance, and there is a reasonable pitching amplitude to make the hovering vertical force optimal. Additionally, the interaction of the tandem configuration will lead to an obvious fluctuation in the aerodynamic force. The research in this paper is helpful to understand the flight mechanism of dragonflies flight.

Keywords: Dragonfly flight, Tandem wings, Interaction, Kinematics, Aerodynamics

1. Introduction

Dragonflies have attracted wide attention for their excellent hovering and fast forward flying ability. The tandem configuration of the dragonfly wing is the main factor that contributes to the remarkable maneuverability. Numerous numerical and experimental researches have been conducted to investigate the aerodynamic performance of the tandem flapping wing like the dragonfly.

Wakeling and Ellington [1] collected the kinematic parameters of dragonfly using a high-speed cine camera during its free-flying condition. Chen et al. [2] and Zou et al. [3] measured the flapping kinematics of dragonflies during the hovering state. They found the wing's flapping movement consists of three-degree-of-freedom motions which are flapping, pitching, and sweeping. Subsequently, the numerical method was implemented to evaluate the aerodynamic performance of dragonflies according to the measured data [4]. Additionally, the flapping kinematics measurement during other flight maneuvers, such as turning [5] and tack-off [6] flight, have also been performed. It is found that the key kinematic parameter like phase shift between forewing and hindwing might vary with the flight maneuvers. According to Nagai et al. [7] who experimentally evaluated the effect of phase angle on the aerodynamic performance of hovering tandem wings, the phase angle of 180° is conducive to stable hovering.

Furthermore, interaction effects between tandem wings also show a potential contribution to the dragonflies' excellent flight performance. Hefler et al. [8] experimentally investigated the flow interactions between forewing and hindwing and asserted a great increase in the circulation of the hindwing leading-edge vortex (LEV). Additionally, their recent result shows that the effect of interaction on the hindwings varies along the wingspan [9]. Maybury and Lehmann [10] investigated the effect of wing spacing and phase shift on the interaction of tandem wings. The research indicated that the force on the hindwing is more sensitive to the spacing and phase shift. Meanwhile, there is a set of optimal vertical spacing and phase shift, which can maximize the lift force and aerodynamic efficiency by forming a reasonable wing–wake interaction [11][12].

Although the wing kinematics of dragonflies during their free flying are already clear at present and the aerodynamic performance of dragonflies in actual flight is preliminarily understood, the effect of the cooperation among each flapping motion on the aerodynamic performance is still unclear. Recent studies have shown that the pitching motion of the tandem wings plays a significant role in weight support of the dragonfly [13][14]. To better understand the relationship between the pitching motion

and flapping motion on the tandem flapping wing, various pitching amplitudes have been numerically investigated during a three dimensional dragonfly-like wing's hovering motion. The instantaneous forces and unsteady flow field around wings are also analyzed. The research in this paper is helpful to understand the flight mechanism of dragonflies and to design a tandem flapping micro aerial vehicle with higher performance.

2. Model and Methods

2.1 Wing model and flapping kinematics

The flapping wing model, consisting of the forewing (FW) and hindwing (HW), used in numerical simulation is obtained from the real dragonfly wings. The length of the forewing and hindwing are 46 mm and 44 mm respectively. The thickness of the wings is 2% of the mean chord length c_f of the forewing. The radius of the second moment of the forewing area R_2 equals 34.3 mm. To mimic the real wing's flapping motion and keep a better mesh quality near the root region, the wing model was configured with a root-cut distance of 0.8c from the flapping axis to the wing root.

As shown in Figure 1, the wings' kinematics combine flapping motion around wing root and pitching motion around a quarter root chord length from the leading edge. Since the amplitude of sweeping motion has been observed to be smaller than that of the other two motions [3], only the flapping and pitching motion are incorporated in this study. Similar to the real dragonfly hovering motion, the FW and HW flap in parallel inclined stroke plane. Meanwhile, the stroke plane angle β, defined as the angle between the stroke plane and the horizontal plane, is equal to 45°. The definition of force vectors on the wing is shown in Figure 2. F_H and F_V are horizontal and vertical forces in the horizontal and vertical plane respectively. L and D are lift and drag forces that are normal and parallel to the stroke plane.

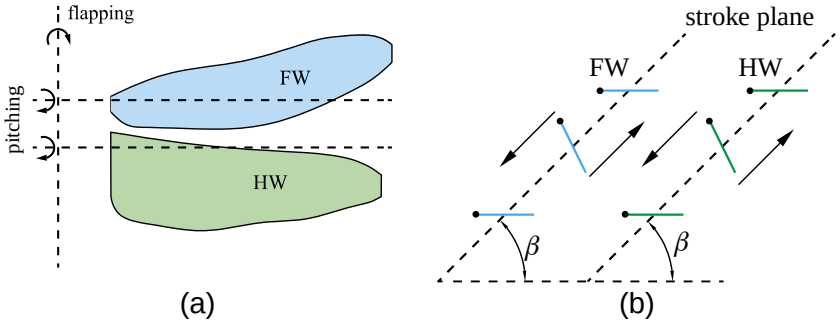

Figure 1 - Schematic of the dragonfly-like flapping model. (a) Definition of flapping and pitching motion; (b) tandem flapping wings trajectory.

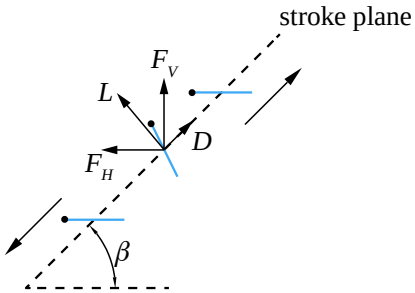

Figure 2 - Definition of force vectors on the wing

The flapping motion of the FW and HW are represented as simple sinusoidal function given by

$$\Psi_f(t) = \Psi_{fm}\cos(2\pi ft) \tag{1}$$

$$\Psi_h(t) = \Psi_{hm}\cos(2\pi ft + \pi) \tag{2}$$

where Ψ_{fm} and Ψ_{hm} is the flapping amplitude of FW and HW and set to 30°, f means the flapping frequency.

The pitching motion of the FW and HW are represented as simple sinusoidal function given by

$$\alpha_f(t) = \alpha_m\sin(2\pi ft) \tag{3}$$

$$\alpha_h(t) = \alpha_m\sin(2\pi ft + \pi) \tag{4}$$

where α_m is the pitching amplitude and α_m of FW and HW is set to the same value in the subsequent simulations. The flapping motion of HW leads the FW by a phase angle of 180°, which has been

proved to be beneficial to stable hovering [15]. And the phase shift between flapping and pitching for both FW and HW keeps at 90°, which is believed to be responsible for high-efficiency flight [16]. The flapping frequency f is equal to 30 Hz. The mean flapping velocity U_{ref} at R_2 is used as the reference velocity in this study and described as:

$$U_{ref} = 4 f \Psi_{fm} R_2 = 2.2\,\text{m/s} \tag{5}$$

The Reynolds number Re can be written as:

$$\text{Re} = \frac{U_{ref} c_f}{v} = 1286 \tag{6}$$

where v is the air viscosity.

2.2 Computational methods

The transient simulations are investigated numerically using the computational fluid dynamics software Fluent by solving the Navier-Stroke equations. The motions of the flapping wings were controlled by a User Defined Function (UDF). The motions of the flapping wings were conducted based on an overset mesh technique. The overset mesh, consisting of background mesh and component mesh, is considered to be suitable for large-scale motion simulation. During the dynamic movement, the background mesh stays stationary, while the entire component mesh moves as a rigid body with the flapping wing controlled by the UDF. Consequently, the component mesh can keep high mesh quality during its movement. The computational domain used for the transient simulations is shown in Figure 3. As can be seen from Figure 3 (a), there are three meshes in total (i.e., two component meshes for each wing and one background mesh for the background zone). For the sake of simplification, only one side of the dragonfly model is simulated. Thus, the symmetric plane is placed at the side of the background mesh. The global size of the background zone is $60c_f \times 50c_f \times 60c_f$. The component zone is characterized by a cylindrical shape with a diameter of 5 times the chord and a height of 2 times the spanwise length of each wing. The background zone is meshed with cartesian grid and each component zone is mesh with unstructured tetrahedral elements, whereas the boundary layer is refined with hexahedral elements. The cell amount of each component mesh is around 1.5 million, and the cell amount of background mesh is around 1 million.

The pressure outlet condition is set to the boundary of the background zone apart from the symmetric plane to simulate the hovering state. The type of the component zone boundary is set to overset. No-slip wall condition is applied to the wing surface. For all the cases in this study, laminar model is adopted to simulate the low Reynold flow situation. Momentum is discretized with second-order upwind scheme. Second-order accuracy is applied to calculate the pressure. The coupled algorithm is employed for the pressure-velocity coupling.

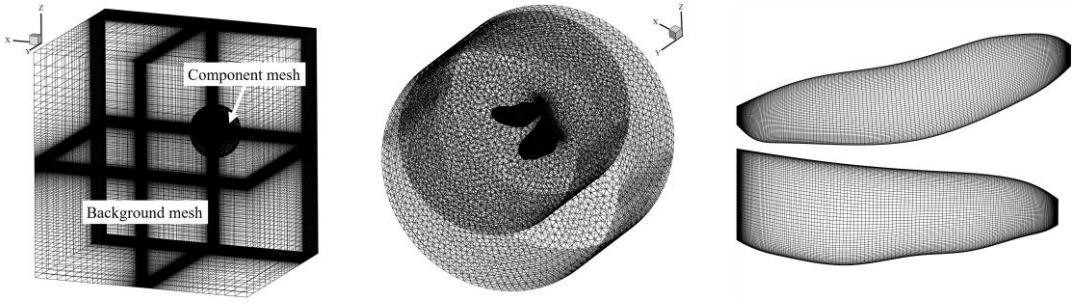

(a) (b) (c)

Figure 3 – Computational setup for the flapping wing. (a) Assembled mesh; (b) component mesh; (c) wing surface mesh.

Dimensionless force data were obtained to analyze the simulation results. The dimensionless force coefficients are given as:

$$C_V = \frac{F_V}{0.5 \rho U_{ref}^2 S} \tag{7}$$

$$C_H = \frac{F_H}{0.5 \rho U_{ref}^2 S} \tag{8}$$

where S is the area of the forewing wing, ρ denotes the density of the fluid.

Time-averaged force coefficient over one flapping period is defined as:

$$\bar{C}_V = \frac{1}{\mathrm{T}}\int_t^{t+\mathrm{T}} C_V(t)\,dt \tag{9}$$

$$\bar{C}_H = \frac{1}{\mathrm{T}}\int_t^{t+\mathrm{T}} C_H(t)\,dt \tag{10}$$

where T is the flapping period.

2.3 Solver validation

The present numerical research is validated with the experiment conducted by Heathcote [17] on a rectangular wing oscillating in pure heave motion. This wing of 600 mm span, 100 mm chord, NACA0012 cross-section was imposed a sinusoidal function at the wing root which described as follows:

$$s = 0.175c\cos(2\pi ft) \tag{11}$$

where s is the displacement of the wing root, f is oscillating frequency. The reduced frequency $k=\pi fc/U_\infty$ is equal to 1.82, where U_∞=0.939 m/s is the freestream velocity.

The topology of the mesh and computational domain is the same as the aforementioned in Section 2.2. The total number of cells for the assembled mesh is around 6 million. Time step in this case is T/200, and the simulation was run for 6 cycles. The thrust coefficient of the last cycle is presented in Figure 4, compared with the experimental data by Heathcote [17] and the numerical result by Liu [18]. It can be found that the results of the present simulation are very close to that of Liu [18]. The trend of the present simulation is in good agreement with the experimental data, with a small discrepancy appearing at the peak and valley values. It should be noted that the inflexible wing in the experiment shows small flexibility rather than a fully rigid wing. This might be responsible for a slight thrust force increase and phase delay, which has also been discussed by Liu [18].

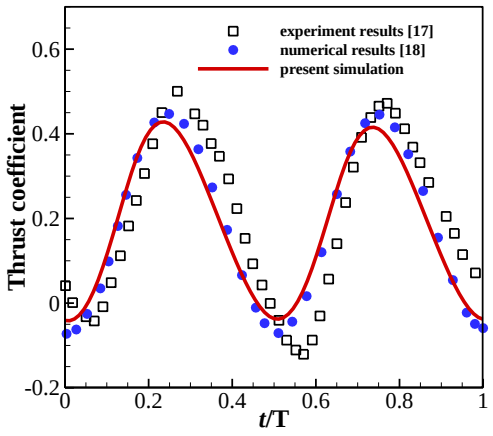

Figure 4 – The thrust force coefficient compared with the reference [17][18].

3. Results and discussion

3.1 Aerodynamic forces

Using the overset mesh method, five different pitching amplitudes (α_m=0°, 15°, 30°, 45°, 60°) were calculated to evaluate the effect of pitching motion on the hovering performance of dragonfly. All cases were computed for six periods and the results of the last period are analyzed.

Figure 5 presents the vertical force coefficient of the tandem flapping wing under different pitching amplitudes in hovering mode. Figure 5 (a) shows the vertical force coefficient of the forewing. Figure 5 (b) gives the vertical force coefficient of the hindwing which leads the forewing by a phase shift of 180°. The gray zone in the diagram means the wing is flapping downstroke. And the light zone indicates the wing is flapping upstroke. The total vertical force coefficient is shown in Figure 5 (c).

As can be seen from Figure 5 (a), most cases can generate peak and valley values during the down and upstroke. Meanwhile, the peak and valley values of these cases almost reach at the same time.

Noteworthy, as the pitching amplitude varies from 0° to 30°, slight change can be found from the magnitude of peak vertical force of forewing. The maximum peak force reaches at α_m=30°. However, when the pitching amplitude continues to increase, the peak value of vertical force during downstroke gradually decreases and changes more gently. During the upstroke, the magnitude of valley value gradually decreases with the increase of pitching amplitude. When α_m is larger than 45°, the forewing can even generate positive vertical force during a small proportion of the upstroke stage. Furthermore, an obvious force platform can be found at t/T=0.25, 0.75. Considering the flapping kinematics, one can found that the distance between the forewing and hindwing is the closest at this moment, which suggests that tandem configuration interaction might account for the force fluctuation.

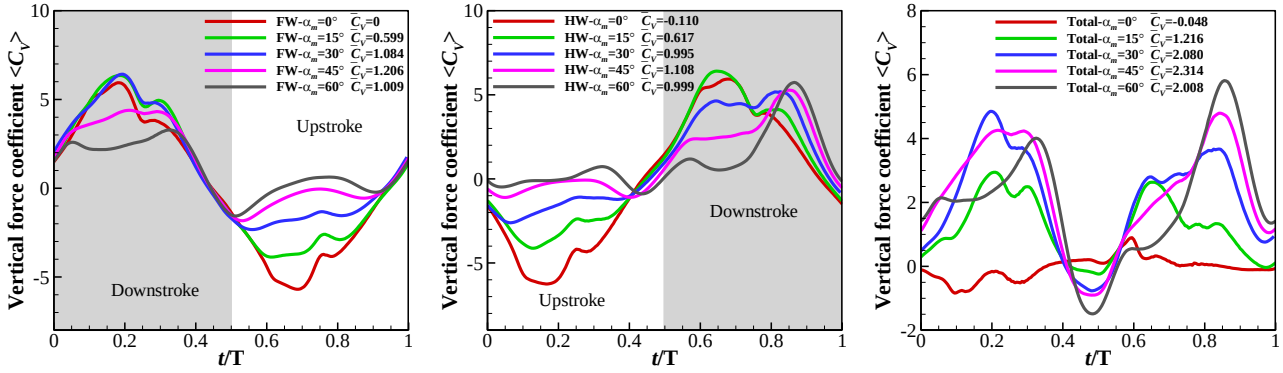

(a) (b) (c)

Figure 5 – Time history of vertical force coefficient under different pitching amplitudes. (a) Forewing wing; (b) hindwing; (c) total wing.

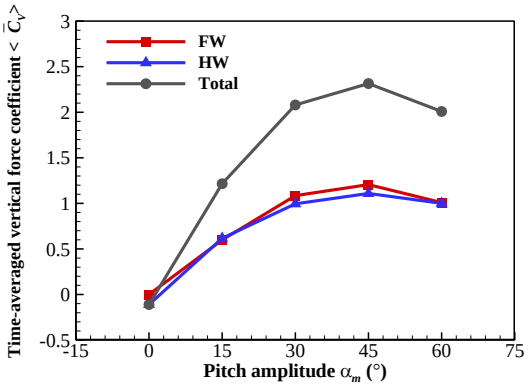

Figure 6 – Time-averaged vertical force coefficient under different pitching amplitudes.

Focusing on the vertical force coefficient of hindwing presented in Figure 5 (b), it is obvious that the force coefficient curves of hindwing also have approximately 180° phase shift compared with that of the forewing. The reason might be the hindwing leads the forewing by a phase shift of 180°. Similar to the force curve trend of the forewing, with the gradual increase of pitching amplitude, the vertical force of the hindwing gradually decreases during its upstroke. When the pitching amplitude is 60°, a small positive peak value occurs at t/T=0.35, and then the vertical force drops rapidly. During the downstroke, the force curves present two peaks, the first peak value happens at t/T=0.65 and the second happens around t/T=0.8. As the pitching amplitude varies from 0° to 60°, the magnitude of the first peak gradually decreases and the second peak gradually increases.

When the forewing and hindwing flaps in counter-phase, two obvious vertical force peaks occur during the tandem wings flapping period by referring to Figure 5 (c), due to the force superposition of the forewing and hindwing. With the implementation of the pitching motion, the tandem wings can generate significantly positive vertical force during a wider proportion of the flapping cycle. When the pitching amplitude increase, the magnitude of peak vertical force also gradually increases, although more obvious negative force will be generated at the timing of stroke reverse (t/T=0.5). The advantages of pitching motion on vertical force generation can be clearly seen from Figure 6. The time-averaged vertical force of both forewing and hindwing goes up as the pitching amplitude increases. When the pitching amplitude reaches 45°, the flapping wing gets the maximum time-

averaged vertical force. After the time-averaged vertical force reaches a maximum, a gentle drop can be observed. This phenomenon suggests that there is a suitable pitching amplitude (α_m=45°) to obtain the maximum hovering vertical force under the tandem configuration.

3.2 Fluid structures

Figure 7 presents the pressure coefficient contour of different pitching amplitudes at the moment of forewing mid-downstroke (*t*/T=0.25). At this moment, the forewing is flapping downstroke and the hindwing is flapping upstroke. It can be clearly seen that there is a low-pressure zone on the upper surface of the forewing nearby the leading edge. Nevertheless, a significant high-pressure zone is observed on the outboard region of the hindwing near the wing tip. With the increase of pitching amplitude, the intensity and size of the low-pressure region on the upper surface gradually increase until α_m=30°. The variation of the low-pressure region implies a strong leading edge vortex has been induced, which might contribute to a high vertical force at this moment by looking at Figure 5 (a). Once the pitching amplitude goes beyond 30°, it is found that the intensity of the low-pressure zone gradually decreases. And even the low-pressure zone can be barely found when α_m=60°, corresponding to the minimum vertical force for the forewing at this moment. This may be because the LEV on the outer part wing has detached and remains a large distance from the wing surface.

As the pitching amplitude varies from 0° to 60°, the high-pressure region on the upper surface of the hindwing substantially reduced, which might be responsible for the monotone decrease of vertical force shown in Figure 5 (b).

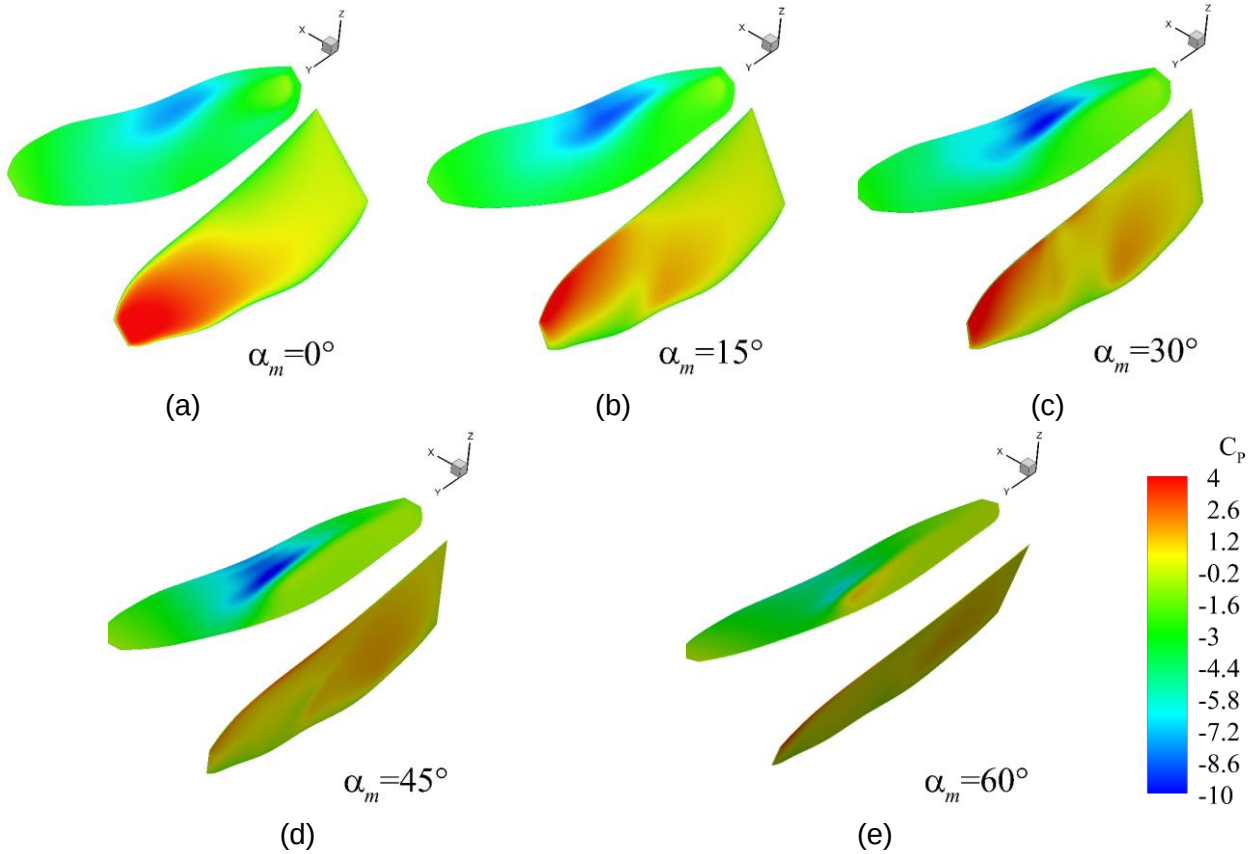

Figure 7 – Pressure coefficient contour of different pitching amplitudes at the moment of forewing mid-downstroke (*t*/T=0.25).

Figure 8 gives a close-up view of vortex contour within the slice at the half spanwise location at *t*/T=0.25. A pair of leading edge vortex and trailing edge vortex (TEV) can be observed around both forewing and hindwing. For the two wings flap in antiphase, the corresponding vortex also presents counter-rotating. As the pitching amplitude increase, the size of the LEV and TEV decrease gradually. Noteworthy, when the pitching amplitude is less than 30°, the LEV on the forewing and hindwing has already lifted off from the wing surface at this time. Although the size of LEV for the case of α_m=0° and α_m=15° is much larger than that for α_m=30°, the detached LEV can not induce enough force exerted on the wing compared with α_m=30°. Additionally, A larger separation region of the LEV might attribute to a lower lift force and rapid decrease of lift by looking at Figure 5 (a). When the pitching

amplitude continues to increase, the local angle of attack of the wings turns to be smaller. Consequently, the size of LEV on forewing and hindwing keep decrease and the LEV starts to remain its attachment to the upper surface for the case of α_m=45° and α_m=60°. Apparently, the LEV with less intensity and size can not induce much suction force, resulting in a lower vertical force magnitude shown in Figure 5.

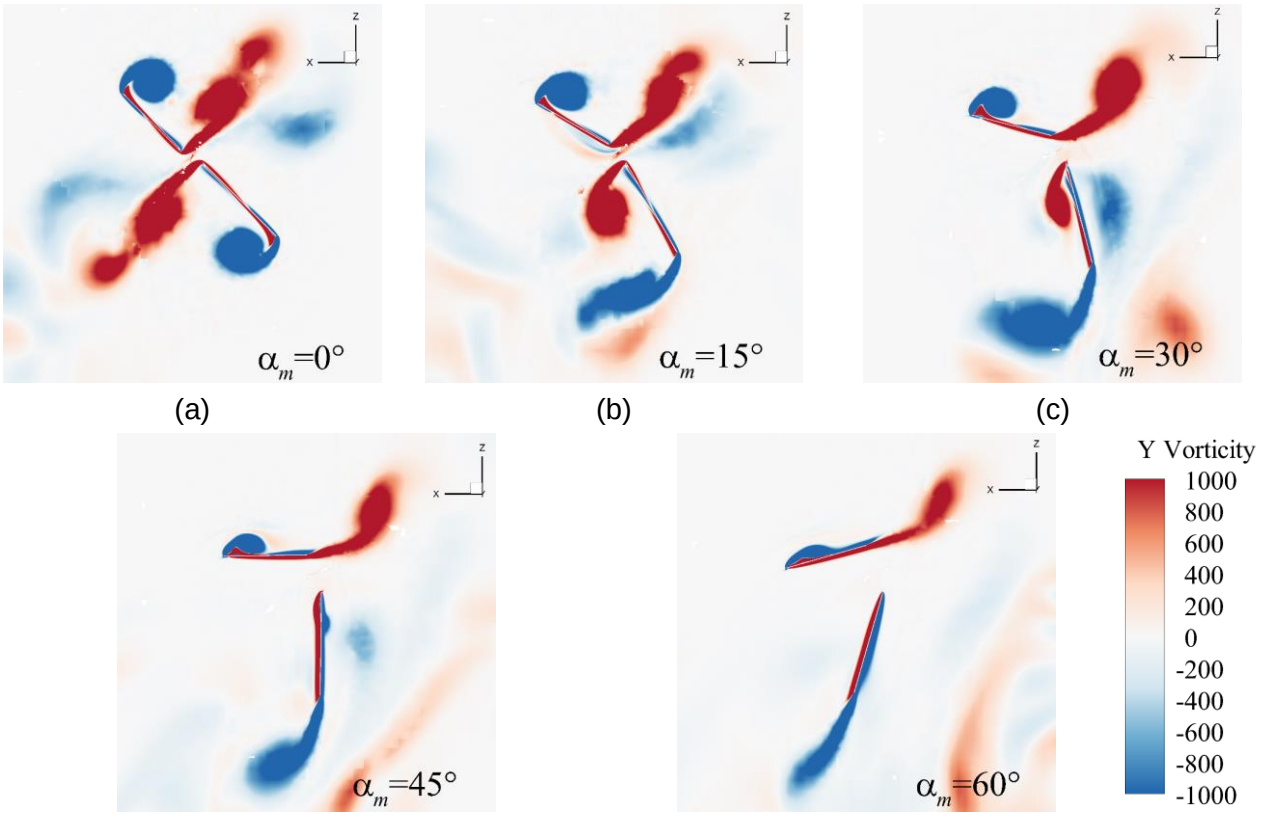

Figure 8 – Vortex contour within the slice at the half spanwise location at the moment of forewing mid-downstroke (*t*/T=0.25).

The interaction between the forewing and hindwing has great impacts on the aerodynamic force of tandem configuration. As can be seen from Figure 8, with the increase of pitching amplitude, the distance between the forewing and hindwing also increases. According to the research by Lehmann and Wehmann [12], the interaction effect between the forewing and hindwing presents gradually attenuation with the increase of the spacing. It is apparent that when the pitching amplitude is small (i.e, α_m=0°), the distance between the tandem wings is close. Therefore, a strong interaction effect leads to a significant force fluctuation by referring to Figure 5. When the pitching amplitude turns to be large (i.e, α_m=60°), the distance between the two wings is far away. Thus, the force fluctuation can be barely seen at this moment due to a weaker interaction effect.

4. Conclusions

In this paper, the aerodynamic characteristics of the tandem flapping wing have been assessed using a numerical method based on the overset mesh technique. Several pitching amplitudes are investigated to evaluate the effects of different pitching kinematics on the aerodynamic performance of the tandem wings. The following conclusions are drawn from the study:

(1) Pitching motion has an apparent impact on the aerodynamic performance of the hovering tandem wings. There is an optimal pitching amplitude to maximize the vertical force when the forewing and hindwing flap in counter-stroking.

(2) Aerodynamic forces on both forewing and hindwing are associated with the interaction of tandem configuration. Meanwhile, the effect of this interaction depends on the distance between the forewing and hindwing. While the space between the two wings decreases, the interaction turns to be stronger, resulting in a force fluctuation exected on the wing.

5. Contact Author Email Address

The contact author email address: langxinyu@mail.nwpu.edu.cn

6. Acknowledgments

This study was supported by the National Natural Science Foundation of China (11872314) and the Key R&D Program in Shaanxi Province of China (2020GY-154).

7. Copyright Statement

References

[1] Wakeling J M, Ellington C P. Dragonfly flight. II. Velocities, accelerations and kinematics of flapping flight. *Journal of Experimental Biology*, 200(3): 557-582, 1997.

[2] Chen Y H, Skote M, Zhao Y, et al. Dragonfly (Sympetrum flaveolum) flight: Kinematic measurement and modelling. *Journal of Fluids and Structures*, 40: 115-126, 2013.

[3] Zou P Y, Lai Y H, Yang J T. Effects of phase lag on the hovering flight of damselfly and dragonfly. *Physical Review E*, 100(6): 063102, 2019.

[4] Chen Y H, Skote M. Study of lift enhancing mechanisms via comparison of two distinct flapping patterns in the dragonfly Sympetrum flaveolum. *Physics of Fluids*, 27(3): 033604, 2015.

[5] Li C, Dong H. Wing kinematics measurement and aerodynamics of a dragonfly in turning flight. *Bioinspiration & Biomimetics*, 12(2): 026001, 2017.

[6] Li Q, Zheng M, Pan T, et al. Experimental and numerical investigation on dragonfly wing and body motion during voluntary take-off. *Scientific Reports*, 8(1): 1-16, 2018.

[7] Nagai H, Fujita K, Murozono M. Experimental Study on Forewing–Hindwing Phasing in Hovering and Forward Flapping Flight. *AIAA Journal*, 57(9): 3779-3790, 2019.

[8] Hefler C, Qiu H, Shyy W. Aerodynamic characteristics along the wing span of a dragonfly Pantala Flavescens. *Journal of Experimental Biology*, 221(19): jeb171199, 2018.

[9] Hefler C, Noda R, Qiu H H, et al. Aerodynamic performance of a free-flying dragonfly—A span-resolved investigation. *Physics of Fluids*, 32(4): 041903, 2020.

[10] Maybury W J, Lehmann F O. The fluid dynamics of flight control by kinematic phase lag variation between two robotic insect wings. *Journal of Experimental Biology*, 207(26): 4707-4726, 2004.

[11] Lehmann F O. Wing–wake interaction reduces power consumption in insect tandem wings. *Experiments in Fluids*, 46(5): 765-775, 2009.

[12] Lehmann F O, Wehmann H N. Aerodynamic interference depends on stroke plane spacing and wing aspect ratio in damselfly model wings. *International Journal of Odonatology*, 23(1): 51-61, 2020.

[13] Liu X, Hefler C, Fu J, et al. Implications of wing pitching and wing shape on the aerodynamics of a dragonfly. *Journal of Fluids and Structures*, 101: 103208, 2021.

[14] Liu X, Hefler C, Shyy W, et al. The Importance of Flapping Kinematic Parameters in the Facilitation of the Different Flight Modes of Dragonflies. *Journal of Bionic Engineering*, 18(2): 419-427, 2021.

[15] Azuma A, Watanabe T. Flight performance of a dragonfly. *Journal of Experimental Biology*, 137(1): 221-252, 1988.

[16] Guglielmini L, Blondeaux P. Propulsive efficiency of oscillating foils. *European Journal of Mechanics-B/Fluids*, 23(2): 255-278, 2004.

[17] Heathcote S, Wang Z, Gursul I. Effect of spanwise flexibility on flapping wing propulsion. *Journal of Fluids and Structures*, 24(2): 183-199, 2008.

[18] Liu H. Integrated modeling of insect flight: from morphology, kinematics to aerodynamics. *Journal of Computational Physics*, 228(2): 439-459, 2009.